Available online at www.CivileJournal.org

Civil Engineering Journal

(E-ISSN: 2476-3055; ISSN: 2676-6957)

Vol. 11, No. 09, September, 2025

Multi-Spring Model and Pushover Analysis of Masonry-Infilled Wall in RC Frame Under Tsunami Loading

Piyawat Foytong [1*], Nuttawut Thanasisathit [2], Teraphan Ornthammarath [3], Supakorn Tirapat [1], Jitrakon Prasomsri [1], Aphidet Nanongtum [1], Anat Ruangrassamee [4], Prinya Chindaprasirt [1]

[1] *Sustainable Infrastructure Research and Development Center, Department of Civil Engineering, Khon Kaen University, Khon Kaen, 40002, Thailand.*

[2] *Department of Civil Engineering, King Mongkut's University of Technology North Bangkok, Bangkok 10140, Thailand.*

[3] *Department of Civil and Environmental Engineering, Mahidol University, Nakornpathom 73170, Thailand.*

[4] *Center of Excellence in Earthquake Engineering and Vibration, Department of Civil Engineering, Chulalongkorn University, Bangkok 10330, Thailand.*

Received 26 June 2025; Revised 11 August 2025; Accepted 19 August 2025; Published 01 September 2025

Abstract

This study investigated the behavior of masonry-infilled walls (MIWs) within reinforced concrete (RC) frames when exposed to hydrodynamic forces from tsunamis by employing a multi-spring modeling approach across different inundation levels. The proposed analytical model divided the MIW into 1 to 5 horizontal nonlinear spring elements that were allocated along the wall's height. Each spring represented a segment of MIW and was defined by a tri-linear force–displacement relationship. The model was calibrated with the experimental data from previous studies and was analyzed using pushover assessment under uniformly distributed hydrodynamic forces corresponding to four tsunami inundation levels (0.25H, 0.50H, 0.75H, and 1.00H). The models, which had employed four or five horizontal springs, had most effectively replicated MIW behavior under tsunami loading at all inundation depths. Conversely, single-spring models tend to overestimate lateral resistance by up to 50%, particularly when the frame is only partially submerged. This discrepancy arises because less force is transmitted through the MIW, with a greater amount of it being transferred directly to the foundation. The utilization of several spring elements provided a realistic load path, improved the interaction between the frame and MIW characterization, and optimized the precision in simulating lateral resistance and post-peak behavior.

Keywords: Masonry-Infilled Walls; Reinforced Concrete Frame; Tsunami Loading; Multi-Spring Model; Pushover Analysis.

1. Introduction

Recent devastating tsunami incidents have highlighted the vulnerability of coastal infrastructure and the need for enhanced structural resilience. The 2004 Indian Ocean tsunami, triggered by a moment magnitude (Mw) 9.1 megathrust earthquake, resulted in over 280,000 deaths in more than 14 nations [1]. The 2011 Tohoku tsunami in Japan, which was induced by a Mw 9.0 earthquake and resulted in over 20,000 fatalities, as well as extensive destruction to essential and residential infrastructure, marked the most catastrophic disaster in Japanese history [2]. Post-disaster reconnaissance has revealed that reinforced concrete (RC) frames with masonry-infilled walls (MIWs) are prevalent in coastal regions, despite having a limited comprehension of their behavior under tsunami-induced hydrodynamic forces.

* Corresponding author: piyafo@kku.ac.th

http://dx.doi.org/10.28991/CEJ-2025-011-09-013

MIWs, previously considered to be non-structural components, have been shown in numerous studies to significantly influence the lateral performance of RC frames. Numerous experimental and analytical studies have confirmed their substantial contribution. Mehrabi et al. [3] performed full-scale cyclic lateral load testing and found that infilled frames had significantly exhibited greater stiffness and lateral strength compared to bare frames. However, they were frequently associated with brittle failure modes, such diagonal compression or shear sliding. Kakaletsis & Karayannis [4] conducted quasi-static cycle testing and found that MIWs had altered the failure process by triggering shear sliding and interface separation, thereby significantly changing the total load path compared to the bare frames. Additionally, through quasi-static and pseudo-dynamic testing, Ozkaynak et al. [5] demonstrated that the incorporation of MIWs had enhanced the energy dissipation capacity of the RC frames, thereby increasing the corresponding damping ratio from approximately 5% in unfilled frames to 12–14% in the infilled counterparts. Asteris et al. [6] conducted numerical simulations to investigate the influence of openings on the behavior of MIW in RC frames and concluded that the existence, dimensions, and placement of openings can significantly diminish lateral stiffness and can alter failure modes, thereby requiring sophisticated modeling techniques to achieve precise representations of these effects.

Various modeling techniques have been proposed to replicate the lateral response of RC frames with MIWs that aim at optimizing computational efficiency while also accurately capturing damage mechanisms. The single-diagonal compression strut model, proposed by Holmes [7], was among the first and most widely utilized models. This simplified approach conceptualizes the MIW as a singular axial compression element that transfers diagonal stresses, making it appropriate for use in preliminary seismic evaluations and code compliance assessments. Nevertheless, the model's assumptions have received increased investigation. Through experimental and analytical investigations, Lee et al. [8] established that although the strut model can be adequately employed to estimate initial stiffness, it fails to capture critical nonlinear phenomena, including interface slip, separation, and progressive damage. To address these limitations, researchers have systematically enhanced the computer simulation of MIWs by implementing multi-strut and multi-spring approaches, which are capable of more accurately representing the dispersed and nonlinear attributes of infill behavior. El-Dakhakhni et al. [9] developed one of the initial advanced models by introducing a three-strut arrangement, wherein a combination of central and corner struts symbolize the MIW. This framework enhances the precision in representing the distribution of lateral stresses and damage processes, including corner crushing and separation, particularly in MIW steel frames. Crisafulli & Carr [10] proposed a refined macro-model for MIWs, incorporating a shear panel element and two diagonal struts to capture both shear deformation and axial compression behavior. The model, which was developed within a nonlinear dynamic analysis framework, demonstrated improved accuracy in simulating strength degradation, stiffness loss, and energy dissipation under cyclic lateral loading when compared to conventional strut models.

Asteris et al. [11] developed a macro-model inside this framework that accommodates infill panels with openings by arranging springs diagonally and vertically along the panel boundaries. This model facilitates a more authentic simulation of localized deformation and interaction effects at discontinuities and provides greater accuracy than conventional single-strut models. Dias-Oliveira et al. [12] utilized a macro-element pattern that integrates multi-segment behavior with the internal subdivision of infill components. This enables the model to reproduce both shear and compressive responses across the panel height, resulting in more accurate estimates of lateral stiffness and post-peak degradation as compared to the single-spring models. Galvão & Alva [13] have introduced a generalized multi-strut modeling approach for RC infilled frames with active MIW, which highlights the calibration of the strut shape and force-transfer mechanisms. To improve modeling accuracy beyond multi-strut and macro-based spring systems, finite element modeling (FEM) techniques have been utilized to clarify complicated failure mechanisms and interface behaviors. Asteris [14] proposed one of the initial micro-models that eliminated the need to assume specific contact zones between the infill and RC frame, thereby facilitating the direct simulation of separation, sliding, and stress transmission. Stavridis & Shing [15] developed nonlinear material models and discrete cracking in mortar joints, which facilitated a precise description of the in-plane deformation and shear failure in concrete. Mohyeddin et al. [16] extended the applications of FEM to simulate coupled in-plane and out-of-plane loading conditions, integrating interface elements that represented separation and damage progression. Baloevic et al. [17] compared macro-FEM and micro-FEM models, revealing that micro-models can accurately depict local behavior, while macro-models can provide computing efficiency for global structural evaluation. Recently, Xi and Liu [18] developed a calibrated FEM that incorporates plasticity-based brickwork behavior, which has subsequently been confirmed through shake-table experiments. Li & Zeng [19] further developed a 3D cohesive interface model that includes dilatancy softening, which enables accurate predictions of cracking, separation, and out-of-plane deformation. Ye et al. [20] conducted finite element analysis using ABAQUS to evaluate the lateral seismic performance of URM walls strengthened with hybrid Basalt–PE Fiber ECCs. Their findings showed improved strength, ductility, and stiffness retention, while reducing brittle failure modes. The study reinforces FEM's role in modeling strengthened masonry infill behavior under lateral loads.

Most existing studies on the behavior of MIWs have focused on seismic loading, in which the lateral forces are generated by inertial effects and are concentrated at discrete mass points, typically at floor levels. Under such loading, the response of MIWs is dominated by high-cycle, dynamic interactions between the infill and the surrounding RC frame. In contrast, tsunami-induced forces exhibit fundamentally different characteristics. Tsunami loads are generally quasi-static, hydrodynamic, and distributed uniformly along the height of the structure up to the inundation depth. These forces arise from a combination of hydrostatic pressure, hydrodynamic drag, buoyancy, and impact forces, and when compared to seismic loads, are applied over a longer duration [21-23]. Despite this apparent difference, relatively few

studies have examined the behavior of MIWs under tsunami loading. Foytong et al. [24] proposed one of the earliest simplified models by representing the infill wall using a single horizontal spring subjected to hydrodynamic pressure. However, their model underestimated the load-transfer mechanisms and as a result, failed to capture the localized damage observed in post-tsunami surveys. To address these limitations, Cavaleri et al. [25] implemented a finite element (FE) modeling framework that includes hydrostatic and hydrodynamic loads and then applied it to evaluate the contribution of MIWs in full-scale RC buildings under tsunami inundation. Building on this work, Del Zoppo et al. [26] highlighted the vulnerability of external infill walls, which tend to fail prematurely and compromise global performance. Belliazzi [27] further extended the modeling strategy by developing a simplified analytical approach that can be used to evaluate building responses under sequential earthquake and tsunami loading. Most recently, Asad et al. [28] have proposed a nonlinear FE-based methodology that can assess MIWs that are subjected to combined in-plane and out-of-plane tsunami-like loads and have explored retrofitting strategies that can mitigate damage. These developments collectively underscore the necessity for infill wall models that can capture the unique characteristics of tsunami forces and their interaction with structural systems.

Although recent studies have explored the behavior of MIWs under tsunami-induced forces, simplified modeling approaches—particularly those based on single-diagonal struts or single-spring representations that were originally developed for seismic loading—are inherently limited in capturing the distinct characteristics of tsunami actions. Unlike earthquake-induced forces, which act at discrete floor levels, tsunami loads are quasi-static and vertically distributed, with maximum intensities near the base of the structure. These simplified models typically assume a uniform lateral force path through the infill, resulting in an unrealistic simulation of load transfer when only a part of the wall becomes submerged. Under such conditions, a significant portion of the hydrodynamic force bypasses the infill and is transmitted directly through the surrounding RC frame to the foundation. This results in inaccurate estimations of lateral strength, energy dissipation, and failure patterns—particularly at the lower inundation depths where the load distribution is highly non-uniform. To overcome the limitations, the present study proposes a multi-spring modeling strategy that discretizes the infill wall into horizontal nonlinear spring components along the height of the RC frame. This configuration enables a more realistic simulation of tsunami pressure profiles, allowing for a detailed investigation into how vertical force gradients can affect infill behavior, failure progression, and lateral resistance. The model offers a practical alternative to more computationally demanding approaches, while significantly improving accuracy over traditional strut-based methods.

The methodology's process is illustrated in Figure 1, which outlines the sequential framework that was adopted in this study ranging from the individual modeling of the RC frame and MIW, through the model calibration and application of the tsunami loads, to the evaluation of structural responses and the development of the proposed modeling scheme. The research began by revisiting the fundamental characteristics of tsunami-induced loads, which differ significantly from seismic forces in terms of uniform pressure distribution. While seismic forces are typically concentrated at discrete floor levels due to inertial effects, tsunami loads increase toward the base and act quasi-statically across the height of the wall, requiring models that can accommodate such gradients. To simulate these conditions, the analysis utilizes an experimentally tested RC frame specimen from previous research as the structural benchmark. This RC frame was modeled using elastic beam elements and plastic hinges at the ends to capture flexural yielding. The infill wall was modeled using a parametric multi-spring configuration, with the number of spring elements ranging from one to five, which were varied along the wall's height. Each spring represented local wall stiffness and post-peak behavior using a tri-linear hysteretic response. The analysis investigated the distribution of forces, failure patterns, and lateral resistance as a function of tsunami inundation depth and spring discretization. The results indicated that enhanced vertical resolution had improved simulation accuracy, especially in detecting failure mechanisms and non-uniform deformation. Ultimately, the study identified an optimal configuration that can balance computational simplicity with accuracy, offering a reliable modeling strategy for assessing MIW vulnerability under tsunami loads.

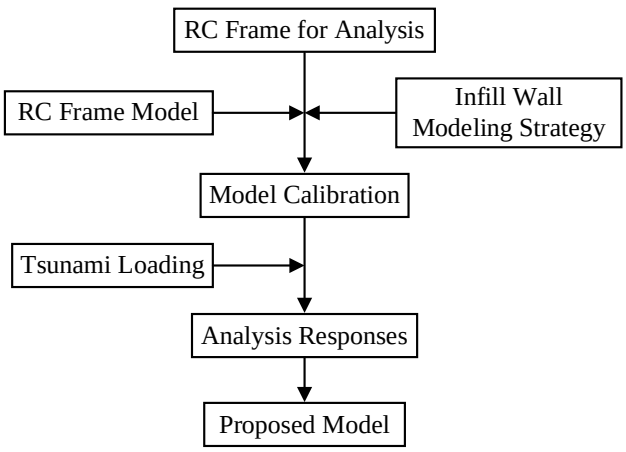

Figure 1. The methodological workflow for the tsunami response modeling of MIW in RC frames

2. Tsunami Loading

Tsunami loading refers to the force exerted on coastal structures by the water during a tsunami event. FEMA P646 [22] specifies different tsunami loading patterns to be included in design calculations. These can be broken down into three main components: hydrostatic, hydrodynamic, and debris impact forces. These forces differ significantly from seismic actions, particularly in their spatial distribution, duration, and fluid–structure interaction mechanisms. The hydrostatic force develops gradually as water moves into a structure. This fluid pressure loading typically applies perpendicular to the surface of the structural and non-structural parts. Due to the pressure difference between the opposite sides of the considered components, this force can cause significant structural damage. In general, hydrostatic forces have a significant effect on long coastal defenses, such as sea barriers. However, the hydrostatic force might not have a substantial effect on low-rise buildings with a relatively short widths, especially when the tsunami inundation rapidly flows and fills entire buildings from all directions.

In contrast to hydrostatic pressure, the hydrodynamic force is the force exerted by the motion of water, which can also cause significant damage to the structure due to the strong flow velocities and vortices generated by the tsunami wave. This dynamic force is a function of fluid density, inundation velocity, and building configuration. Based on ASCE [29], the hydrodynamic forces are required to be considered for the whole structure and each structural component that is submerged under the water. Also recognized as a drag force, there are differences in approximating the value of hydrodynamic forces. In general, the drag force (F_D) can be estimated as recommended by FEMA 55 [30] and CCH [31] by following the formulation as shown in Equation 1:

$$F_D = \frac{1}{2} C_D A \rho u^2 \quad (1)$$

in which F_D is hydrodynamic drag force, C_D is drag coefficient (dimensionless), ρ is fluid density, u is flow velocity, A is the projected area of the element perpendicular to the flow direction

Based on FEMA 55 [30] and CCH [31], the drag coefficient of 2.0 is assigned for square columns with damaged non-structural walls. Conversely, for undamaged structural walls, the drag coefficients are 1.25 and 1.50 for FEMA 55 [30] and CCH [31], respectively. The impact force is the force generated by the impact of the water on the structure. It can cause significant damage to the structure due to the high momentum transfer and dynamic pressure, which is exerted on the building [30]. Impact forces are a function of the weight of the debris, the flow depth, and the maximum flow velocity carrying the debris. In general, the debris impact forces are expected to occur independently of other tsunami loadings. The appropriate force model for simulating the behavior of tsunami-induced forces on buildings is the hydrodynamic force model, which is the uniformly distributed force throughout the water depth [21-23]. Therefore, this study focused on evaluating the effects of hydrodynamic forces induced by tsunami flow on buildings.

3. Frame for Analysis

The RC frame model used in this study was based on Specimen No. 8 from the experimental program conducted by Mehrabi et al. [3], which served as a validated reference for simulating the lateral behavior of MIW in RC frames. This specimen comprised a single-bay, single-story RC frame with a column height of 1.40 meters and a clear span of 2.90 meters, which represents the typical configurations of low-rise residential structures in coastal areas [32]. The columns include a cross-sectional area of 175 mm x 175 mm, reinforced with 8 DB12 longitudinal bars and RB6 stirrups at 75 mm intervals. The beam features a cross-section of 150 mm by 225 mm, strengthened with four DB16 longitudinal bars and RB6 stirrups at 75 mm intervals. An axial load of 293 kN was consistently delivered to replicate the effects of gravity. The material qualities of the frame components were obtained from the original experiments. The concrete had a compressive strength of 30.9 MPa and an elastic modulus of 21.9 GPa. Reinforcing steel demonstrated yield strengths of 413.7 MPa (DB16), 420.6 MPa (DB12), and 367.5 MPa (RB6), accompanied with an elastic modulus of 200.6 GPa. The MIW consisted of solid clay bricks with mortar joints with a thickness of 9.21 mm. The compressive strengths of the brick and mortar were 16.5 MPa and 15.5 MPa, respectively. The masonry prism revealed a compressive strength of 9.5 MPa and a modulus of elasticity of 5.1 GPa. These properties were utilized for model calibration in order to provide an accurate simulation of MIW response under tsunami-induced lateral loading.

4. Model and Calibration

This study utilized a theoretical framework to analyze the combined interactions between MIWs and RC frames in response to the spatially distributed hydrodynamic forces induced by tsunamis, as illustrated in Figure 2. Tsunami forces, in contrast to seismic excitation, which induces lateral strains at specific story levels through inertial effects, impose a quasi-static impact that is equally distributed across the structure's height, exceeding the inundation depth. This distribution necessitated a modeling approach that was capable of accurately modeling the vertical stress variation, the frame-infill interaction at different elevations, and the progressive failure mechanisms across the height of the wall. The RC frame was modeled using elastic beam elements that incorporate nonlinear plastic hinges at the beam and column extremities to represent flexural yielding, in accordance with the moment–curvature relationship defined by ASCE 41-

13 [33]. Column elements were divided at each spring level to depict the localized interaction between the infill and the frame, allowing for the incorporation of additional hinges to address any localized plasticity near the spring interfaces. This segmentation improves the ability of the model to simulate deformation compatibility and interaction forces between the MIW and RC frame, especially under non-uniform horizontal loads. To ensure consistent and realistic force transmission between the springs and the frame, rigid links were used to connect the spring nodes to the RC frame. The total lateral force of the infill was appropriately distributed throughout the spring components, facilitating the model to simulate the gradual interaction. The number of springs employed in the model was modified to investigate the effects of horizontal precision on structural response. This parametric study examined the impact of discretization on key outcomes, including global lateral resistance, damage localization, and interface separation, particularly under the conditions of partial or complete submersion.

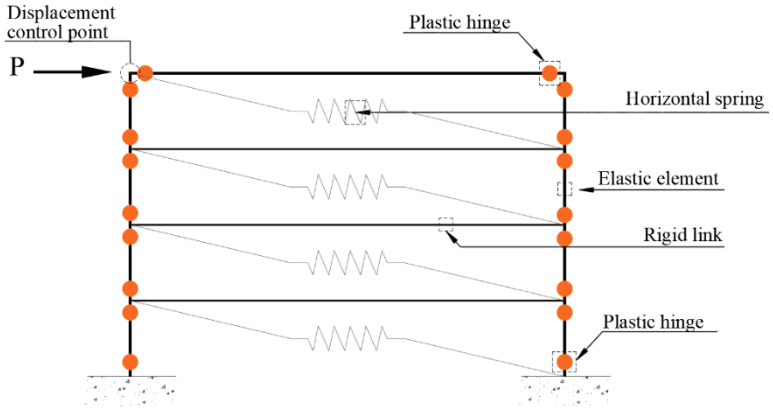

Figure 2. The components of the MIW model in the RC frame using four springs

The MIW is represented by a sequence of horizontally arranged nonlinear spring elements, each representing a particular elevation of the infill segment. This multi-spring modeling technique enables the simulation of localized deformation, interface separation, and unbalanced force distribution under tsunami loading conditions. Each spring demonstrates a simplified trilinear force-deformation relationship, which is subdivided into four stages: initial elastic response, yield, post-yield softening, and residual strength that were proposed by Mostafaei & Kabeyasawa [34]. The maximum lateral resistance of each spring is determined by the lower capacity of two fundamental in-plane failure modes—diagonal compression and sliding shear, which are defined by wall aspect ratio, material strengths, and boundary conditions at the interface.

MIWs primarily transfer lateral forces by establishing a compression strut diagonally between the opposing corners of the RC frame. This diagonal compression mechanism illustrates the infill's attempt to resist lateral deformation by establishing a compression field that is associated with its diagonal axis. Consequently, the majority of the lateral load is countered by this internal diagonal strut, which can endure axial compression stress while transferring the force to the surrounding RC frame. To incorporate diagonal compression behavior into simplified models, the compressive strength of the infill panel can be evaluated by idealizing the diagonal compression strut and applying a force equilibrium formulation as demonstrated in Equation 2.

$$V_C = f_m t_w w_e cos\theta \tag{2}$$

in which V_C is lateral strength due to diagonal compression, f_m is compressive strength of masonry, t_w is thickness of the infill wall, w_e is equivalent strut width, θ is angle of diagonal strut.

Sliding shear failure is a prevalent in-plane failure mechanism in MIWs, especially when the bonding at the interface between the masonry units or between the infill and the RC frame is inadequate, or when the shear load exceeds the frictional resistance of the mortar joints. In contrast to diagonal compression failure, which simulates compressive strut action along the diagonal, sliding shear failure involves relative movement along the horizontal mortar joints, typically located at the mid-height of the wall. This failure mechanism occurs when the lateral force reaches the frictional capacity of the masonry bed joints or the interface shear strength at the connection between the infill and the RC frame columns. Cracking at the horizontal joints or interfaces results in the wall sliding as a rigid body, causing a reduction in strength and stiffness. The sliding shear capacity of the infill wall can be expressed using a Coulomb-type friction model, which integrates cohesion and frictional resistance, as described in Equation 3.

$$V_{sl} = \tau_0 t l_m + \mu N \tag{3}$$

in which V_{sl} is lateral strength due to sliding shear, τ_0 is shear stress capacity at the mortar interface, l_m is length of infill wall, μ is coefficient of friction between masonry materials, N is normal force acting on the sliding plane.

The MIW's behavior within the RC frame was verified using experimental data from Mehrabi et al. [3], who provided reference measurements of the lateral load-displacement response. The present research modeled the MIW using a discrete multi-spring approach, in which the infill panel was depicted as a sequence of horizontally aligned nonlinear springs. Five configurations were developed by varying the number of spring elements from one to five along the height of the panel, as illustrated in Figure 3. The lateral force-deformation response of each spring was represented by a trilinear hysteretic model with three phases: initial yielding (V_y, U_y), peak lateral resistance (V_m, U_m), and post-peak residual resistance (V_p, U_p). In addition, as summarized in Table 1, the model included the diagonal strut angle (θ) and the stiffness (K) of each spring, which were calculated based on the geometric segmentation of the MIW panel. Calibration was performed through a series of displacement-controlled pushover analyses, in which lateral loading was applied at the top-left node of the frame to replicate the test setup.

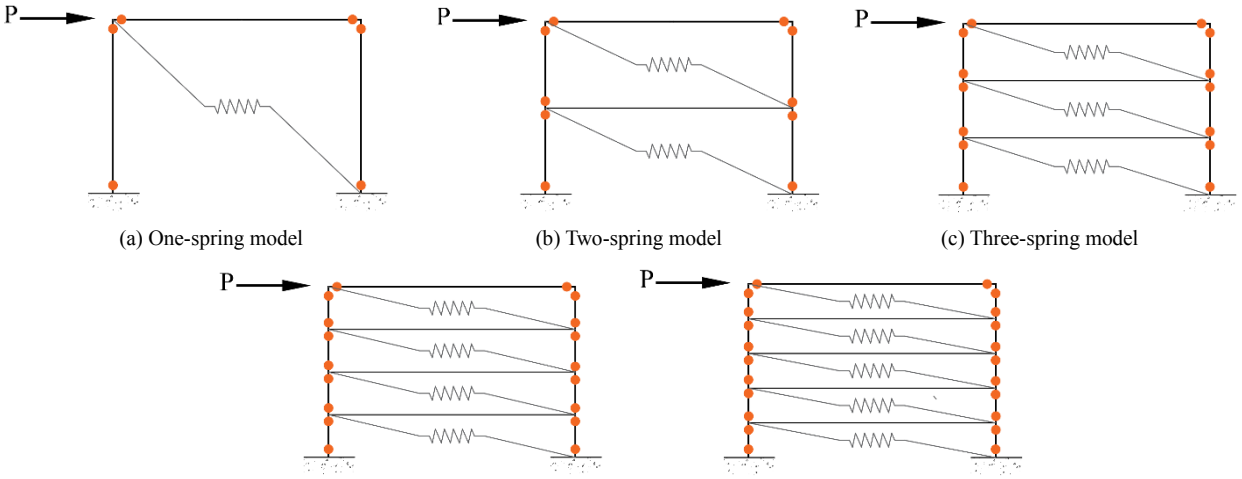

(a) One-spring model (b) Two-spring model (c) Three-spring model

(d) Four-spring model (e) Five-spring model

Figure 3. The multi-spring model of the MIW under tsunami loading

Table 1. The spring element properties of the MIW models

Models	θ (Degree)	Lateral resistance (kN)			Lateral Displacement (mm)			K (kN/mm)
		Yielding	Max	Residual	Yielding	Max	Residual	
		(V_y)	(V_m)	(V_p)	(U_y)	(U_m)	(U_p)	
1-Spring	33.70	126.50	168.66	50.60	2.60	6.92	37.89	33.731
2-Springs	18.40	110.91	147.88	44.37	2.28	6.07	14.18	43.850
3-Springs	12.50	107.80	143.73	43.12	2.22	5.90	6.35	46.361
4-Springs	9.50	106.70	142.27	42.69	2.19	5.84	6.41	47.405
5-Springs	7.60	106.17	141.56	42.47	2.18	5.81	6.44	47.836

The comparison between the numerical results of the multi-spring MIW models and the experimental data from Mehrabi et al. [3] is illustrated in Figure 4. All spring configurations demonstrated consistent behavior within the linear range of the test results. However, significant discrepancies occurred in the post-yield region. Models incorporating the three to five spring elements exhibited improved agreement with both the peak lateral resistance and the subsequent softening behavior, indicating a more accurate representation of damage progression and residual strength. The one-spring model overestimated the peak resistance and inadequately simulated the post-peak degradation, whereas the five-spring model slightly overestimated the post-peak resistance. In contrast, the two-spring and four-spring models marginally underestimated the peak strength. This comparison highlighted that the number of spring elements can significantly influence both stiffness distribution and damage localization. By capturing the horizontal variation of the force distribution and interface behavior, the three-spring and four-spring models provided an optimal trade-off between modeling accuracy and computational efficiency. Notwithstanding the differences in specifics, they successfully captured the general behavioral trend of the tested specimens under lateral loading. This validated the reliability of the multi-spring modeling approach for simulating the behavior of MIWs in RC frame structures.

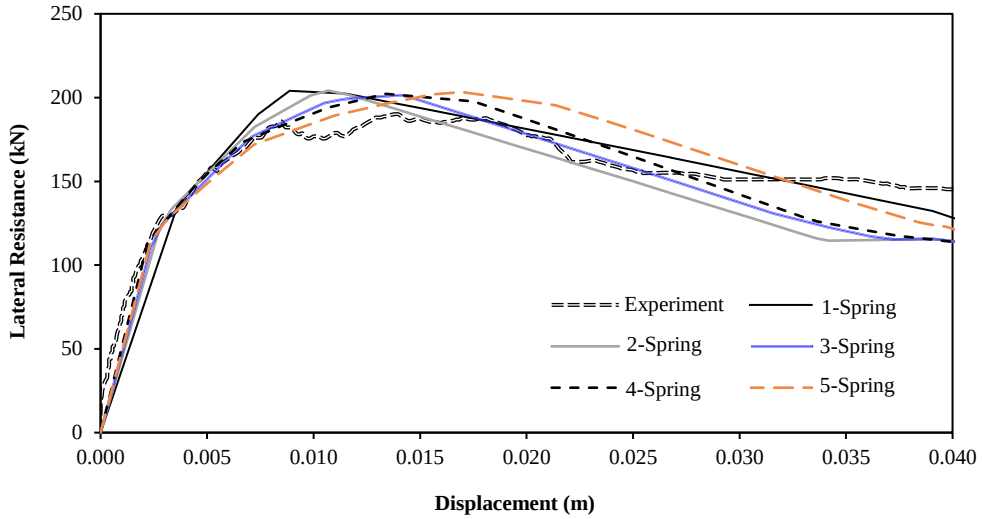

Figure 4. A comparison of the analytical results vs. the experimental results of the study by Mehrabi et al. [3]

5. Analysis and Modeling of Masonry-Infilled Wall

The structural behavior of MIW subjected to tsunami-induced lateral forces was investigated using a simplified numerical model composed of multiple horizontal spring elements. A nonlinear pushover analysis was performed by applying a uniformly distributed load to simulate the hydrodynamic pressure that would be exerted by a tsunami wave. The tsunami loading was represented by fixing the spatial distribution of pressure to match the inundation depth, while the loading magnitude was gradually increased by controlling the flow velocity, following a displacement-controlled procedure. The velocity range was defined between $0.7\sqrt{gh}$ and $2.0\sqrt{gh}$, which was based on FEMA55 [30], Fritz et al. [35], and Foytong et al. [36], in which g is the gravitational acceleration and h is the inundation depth. To evaluate the influence of the inundation levels on the MIW response, four depths were considered: 0.25H, 0.50H, 0.75H, and 1.00H, in which H represented the total height of the RC frame.

The infill wall was modeled using 1 to 5 discrete horizontal spring elements, which reflected the nonlinear lateral stiffness and strength degradation of the MIW. The configuration of the RC frame and the applied tsunami loading conditions are illustrated in Figure 5. The pushover analysis was continued until global instability had occurred, which was triggered either by the failure of the spring elements representing the MIW or the formation of a plastic hinge in the RC columns. To capture the post-peak softening behavior, the model allowed for continued analysis beyond the peak lateral resistance. The lateral resistance was calculated as the sum of the shear forces at the fixed supports at the base of the columns.

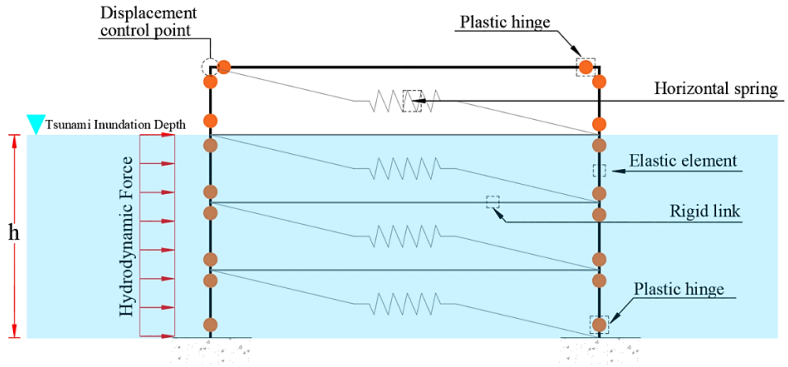

Figure 5. The tsunami force acting uniformly on the MIW in the RC frame model

5.1. Tsunami Inundation Depth of 0.25H

The behavior of MIWs within the RC frames, which was subjected to tsunami-induced lateral loading at an inundation depth of 0.25H, exhibited a pronounced sensitivity to the number of horizontal spring elements used to model the infill. As shown in Figure 6, this discretization had a significant influence on the correlation between the lateral resistance and the resulting deformation. Complementing this, Figure 7 illustrates the progression of failure mechanisms across the varying spring configurations. The numerical labels indicate the sequential order of yielding for each structural component. Labels at the column locations represent plastic hinge formation, while those adjacent to springs denote yield in the corresponding masonry segments. All comparisons were made under the condition of equal maximum lateral resistance across models in order to isolate the effect of spring discretization.

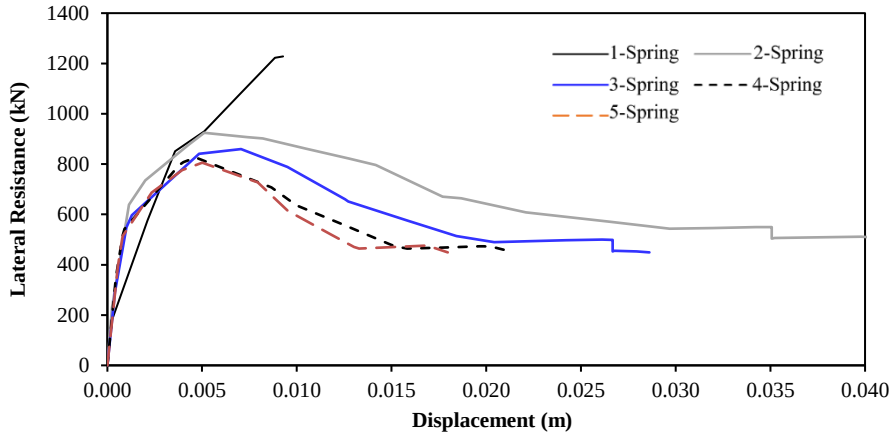

Figure 6. The relationship between the lateral resistance and deformation of the MIWs in RC frames that were subjected to tsunami inundation depths of 0.25H

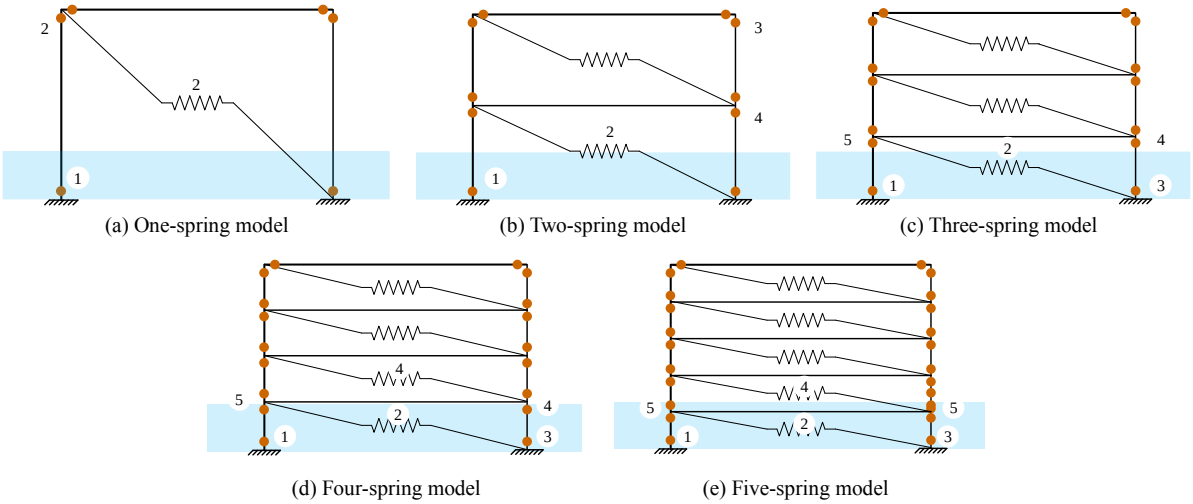

Figure 7. The failure mechanisms of the MIW models that were subjected to tsunami inundation depths 0.25H

In the single-spring model, failure was significantly confined and governed mainly by the frame. The mechanism initiated with the development of a plastic hinge at the base of the front column, which was concurrently accompanied by yielding in the spring element representing the infill and the formation of a hinge at the top of the same column. The lack of vertical resolution in the infill model prevented realistic interaction with the hydrodynamic pressure profile of the tsunami. As a result, the majority of the applied force was transmitted directly through the front column to the foundation, entirely bypassing the infill wall. This resulted in an overestimated assessment of lateral stiffness and strength, with the model demonstrating a maximum peak lateral resistance of 1,228.0 kN, despite minor input from the infill. The resultant response thus demonstrated a focused force path through the frame instead of a dispersed contact between the MIW and the structural components. The two-spring model introduced a slight increase in complexity. Following the formation of a hinge at the base of the front column, yielding developed in the lower spring, followed by plastic hinges at the upper and mid-height sections of the rear column, close to the rigid link. Although the infill transferred some loads, the wide spring spacing continued to limit interaction with the vertical distribution of the tsunami forces. Consequently, the peak lateral resistance dropped to 924.5 kN, which indicated only a partial contribution.

As the number of springs increased to the three-spring model, the failure mechanism became more distributed and physically realistic. In this model, the progression began at the front column base, which was followed by yielding in the bottom spring, yielding at the rear column base, plastic hinge formation at the mid-height of the rear column, and ultimately, deformation at the lower joint of the front column. This sequence reflected a more balanced load-sharing between the frame and the infill, with the internal forces being redistributed across multiple components. The maximum lateral resistance decreased to 858.6 kN. The four-spring model extended this trend with greater refinement: the failure began at the front base, continued through the lowest spring, initiated hinge formation at the rear column base, induced yielding in the second infill level, and concluded with plastic hinge formation in both columns at the lower rigid link. The improved vertical discretization enabled a more realistic simulation of progressive wall degradation and a more accurate interaction with the RC frame. The corresponding resistance was reduced to 825.2 kN. The five-spring type provided the most advanced and physically precise failure pattern. It initiated with a plastic hinge at the base of the front

column, followed by yielding in the lowest spring segment. A hinge then formed at the base of the rear column, indicating that the frame participated on both sides. Yielding next occurred in the second spring segment, showing the infill wall's layered response. The final stage involved the simultaneous formation of plastic hinges at the rigid link connections in both the front and rear columns, reflecting balanced load transfer and coordinated failure across the RC frame. With its finer vertical resolution, this model accurately captured the gradient of tsunami-induced hydrodynamic pressure and internal force redistribution, which resulted in a peak lateral resistance of 805.1 kN, the lowest among all configurations, yet the most physically representative. The comparison research indicated that although low-resolution models may exhibit greater lateral capacities, this phenomenon resulted from unrealistic force routes that had bypassed the infill wall and had pushed loads into the RC frame, particularly through the front column to the foundation. In contrast, models using four or five spring elements had been able to more precisely allocate the applied tsunami forces throughout the infill and adjacent RC elements, facilitating progressive failure and interaction that aligned with real behavior. Beyond the three-spring threshold, the lateral resistance values and load-displacement responses began to converge, indicating that beyond this point, further refinement of the springs offers diminishing returns in predicting global behavior.

5.2. Tsunami Inundation Depth of 0.50H

The structural performance of the MIWs within RC frames subjected to tsunami-induced lateral stresses at a water inundation depth of 0.50*H* demonstrated the impact of vertical discretization on the overall resistance and localized failure behavior. Figure 8 illustrates that the variations in the number of horizontal spring elements utilized to simulate the infill wall had considerably influenced the force–displacement response. Figure 9 identifies the development of structural damage among the various spring configurations. All models were assessed under the same loading conditions in order to provide an equal comparison that focused primarily on the effects of spring resolution.

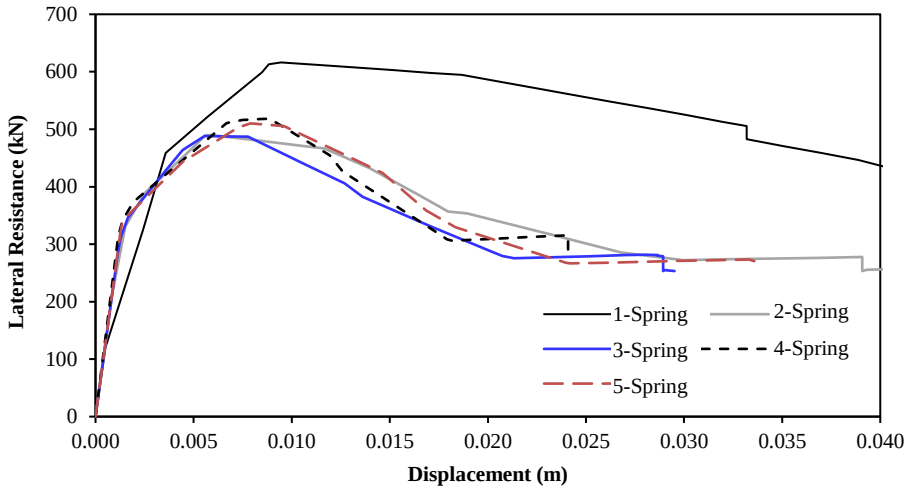

Figure 8. The relationship between the lateral resistance and the deformation of MIWs in RC frames that were subjected to tsunami inundation depths of 0.50H

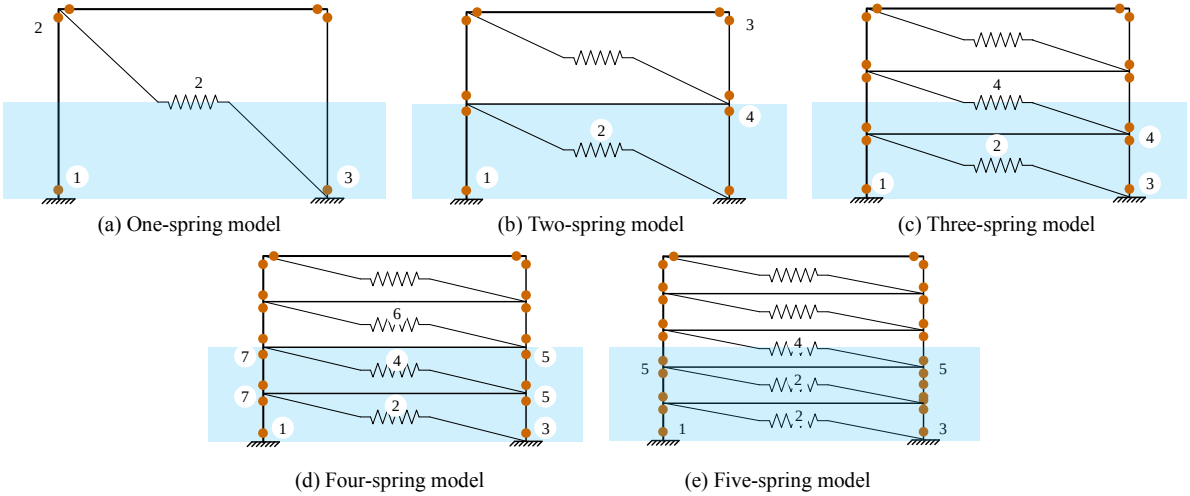

Figure 9. The failure mechanisms of the MIW models that were subjected to tsunami inundation depths of 0.50H

The single-spring model exhibited a straight and concentrated failure path, primarily controlled by the frame. Yielding started with a hinge at the base of the front column, followed by simultaneous yielding in the spring and the formation of a top hinge within the same column. Damage later extended to the rear column base, signifying greater frame involvement due to the higher inundation level. This configuration demonstrated a maximum lateral resistance of 616.0 kN, which was primarily due to the infill wall, depicted by a single spring that had failed to contribute significantly to load distribution. As a result, the applied force was predominantly transferred through the RC columns directly into the foundation. In the two-spring model, the response had slightly more distribution. Yielding initially occurred in the lower spring after the front base hinge, which was followed by hinge development at the upper and mid-height sections of the rear column. Nevertheless, a solitary spring remained submerged, limiting interaction with the tsunami pressure gradient and decreasing the peak resistance to 489.7 kN. The incorporation of additional spring elements enabled the models to depict more complex damage patterns and realistic force redistributions.

In the three-spring arrangement, failure commenced at the front column base, progressed through the lowest spring, and then expanded to the rear column base and mid-height rigid link, which was accompanied by yielding in the middle infill segment. This resulted in a slightly reduced peak resistance of 487.0 kN, highlighting the persistent limitation imposed by the presence of only a single or partially submerged spring at the loading depth. The four-spring model exhibited a more pronounced enhancement in accurately representing the hydrodynamic force transfer. Two springs were entirely situated within the inundation zone, facilitating enhanced interaction with the infill. The failure sequence became more complex, exhibiting yielding at both lower spring levels and hinge creation at various sites within the front and back columns, especially near the connections. This enhancement enabled the system to absorb and redistribute forces more efficiently, resulting in a resistance of 518.0 kN. In the five-spring model, the behavior progressed, beginning with the base yielding at the front column, followed by sequential yielding at the two lowest spring segments and yielding in the third spring, as well as the concurrent construction of hinges at both second-level rigid links. This model, which featured a denser spring network, achieved a maximum resistance of 510.2 kN, indicating an enhanced modeling of force distribution across the wall's height.

These findings confirmed that enhanced spring resolution can elevate the accuracy of simulated tsunami loading effects. Although lower-resolution models may exhibit inflated resistance values, these are often deceptive due to the overestimated concentration of loads within the RC frame and the negligible contribution from the infill. Conversely, multi-spring models—particularly those with four or five elements—facilitate more dispersed damage and enhance the portrayal of structural interactions. The minor differences observed between the four-spring and five-spring models indicated a convergence in global response beyond a specific threshold of vertical discretization. In contrast, localized behavior retains the advantage of enhanced resolution.

5.3. Tsunami Inundation Depth of 0.75H

The structural response of MIWs in RC frames subjected to tsunami-induced lateral forces at an inundation depth of 0.75*H* demonstrated a significant reliance on the vertical discretization of the MIW components. Figure 10 illustrates the correlation between the quantity of the spring elements and the lateral resistance, whereas Figure 11 depicts the associated failure causes for each model configuration. In the one-spring model, the failure mechanism was primarily dictated by frame action. The sequence initiated with the establishment of a plastic hinge at the base of the front column, followed by yielding in the infill spring, the construction of an upper hinge at the front column head, and ultimately, yielding at the rear column base. Despite this localized damage, the model achieved a maximum lateral resistance of 439.1 kN, primarily due to the total submersion of the spring and the concentrated force transmission. The two-spring model exhibited a comparable trend, with slightly more dispersed failure: the damage was initiated at the front base, progressed through the lower spring, and then extended to the top and mid-height links of the rear column, reducing the resistance to 370.2 kN. The three-spring model illustrated an enhanced failure resolution, starting with yielding in the lowest spring, followed by simultaneous hinge creation at both column bases, subsequent yielding in the middle spring, and then culminating in hinge formation at the rear link interface. This configuration resulted in a resistance of 384.2 kN, indicating a more proportionate distribution of force.

The four-spring model delineated an advanced failure sequence comprising six discrete stages. Damage, which initiated with yielding in the second spring and progressed to the lowest spring and the front column base, led to hinge formation at the rear column base, which resulted in yielding in the third spring, and culminated in the construction of plastic hinges at both sides of the stiff mid-height link. The corresponding maximum lateral resistance increased to 398.0 kN, indicating improved structural interaction. The five-spring model provided the most realistic simulation. The mechanism began with yielding in the second spring, subsequently advancing to the lowest spring, the front base hinge, the rear column base hinge, and then to the failure of the third spring, which

ultimately resulted in concurrent plastic hinges at the second link level of both columns. This system achieved a resistance of 406.1 kN, the greatest among the multi-spring models, and precisely depicted the gradual and distributed characteristics of tsunami-induced failure. The incorporation of increasing spring elements enhanced the vertical resolution, enabling the model to more precisely describe the gradient of hydrodynamic forces and the complex interactions between the infill wall and the adjacent RC frame. While the maximum lateral resistance typically diminishes or stabilizes after the two-spring setup, the simulated failure mechanisms are increasingly detailed and realistic. This improved fidelity offers a more robust and reliable basis for the structural evaluation of MIW in RC frames when subjected to tsunami-induced loading conditions.

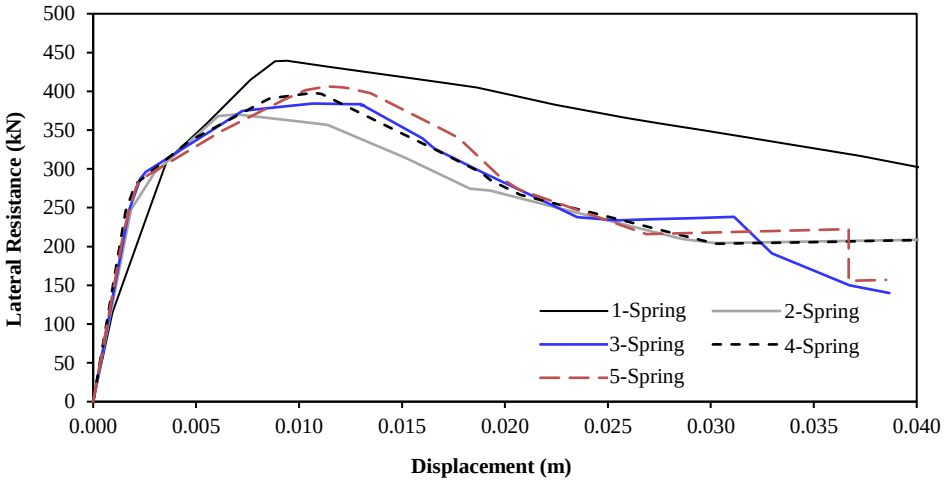

Figure 10. The relationship between lateral resistance and deformation of the MIWs in RC frames that were subjected to tsunami inundation depths of 0.75H

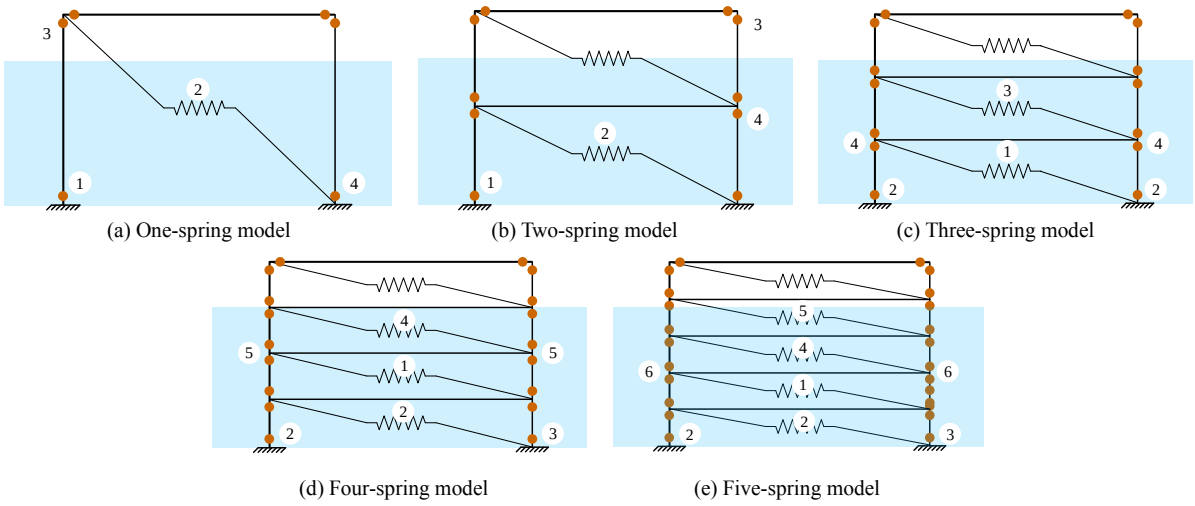

Figure 11. The failure mechanisms of the MIW model that was subjected to tsunami inundation depths at 0.75H

5.4. Tsunami Inundation Depth of 1.00H

The behavior of MIWs within RC frames under tsunami-induced lateral stress at an inundation depth of 1.00H was closely related to the quantity of horizontal spring elements that were used to model the infill response. Figure 12 illustrates that the maximum lateral resistance across all configurations exhibited a converging trend, with the single-spring model achieving the maximum resistance of 352.2 kN. Nonetheless, this figure was only slightly higher than those reported in the multi-spring models, which had exhibited peak resistances of 319.3 kN, 329.5 kN, 339.2 kN, and 343.8 kN for the two-spring, three-spring, four-spring, and five-spring configurations, respectively. The post-peak behavior of the single-spring model exhibited accelerated stiffness decay, but the multi-spring setups displayed more gradual and physiologically realistic responses. This tendency arose from the complete submersion of all the spring segments under the 1.00H inundation depth, enabling the multi-spring models to more precisely represent the vertical gradient of hydrodynamic loading and to appropriately allocate the internal forces.

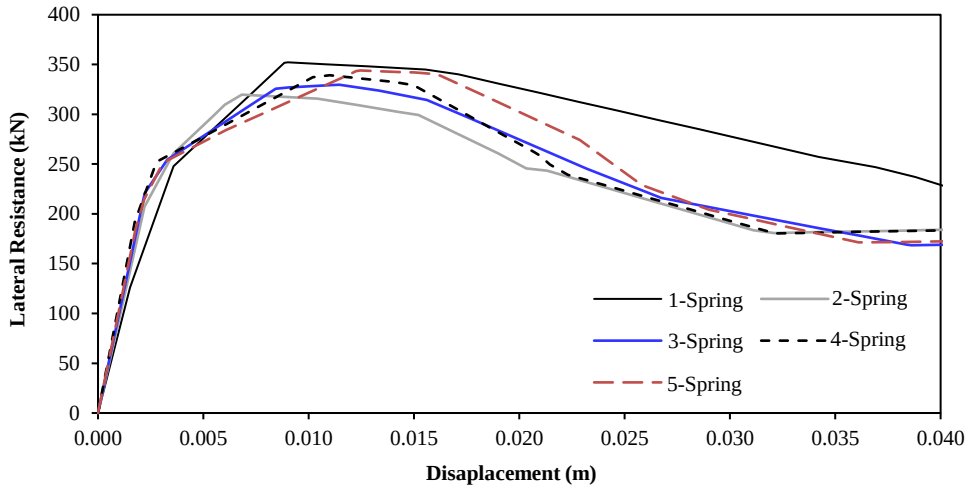

Figure 12. The relationship between the lateral resistance and the deformation of the MIWs in RC frames that were subjected to tsunami inundation depths of 1.00H

The failure processes depicted in Figure 13 further validated these patterns, demonstrating the incremental nature of damage in setups with increased spring discretization. In the single-spring model, failure commenced with the formation of a plastic hinge at the base of the front column that was succeeded by yielding in the infill spring and the development of a plastic hinge at the rear column base, which signified focused force transmission into the frame. Conversely, the two-spring model demonstrated layered damage, initiating with the yielding of the lower spring, simultaneous hinging at both columns, and subsequent yielding in the top spring. The three-spring model demonstrated failure beginning in the lower and middle springs, with plastic hinges developing at the base of the front column and the top of the rear column, signifying an enhanced distribution of the damage. In the four-spring design, cracking advanced sequentially through the lower three spring layers, which was accompanied by the development of hinges at both column bases.

The five-spring model exhibited the most extensive damage course, characterized by sequential failure over the five infill layers and concurrent yielding at both column bases, indicating a balanced interaction and force redistribution inside the structure. The enhancement in the peak lateral resistance diminished after two or three spring elements, although the fidelity of the failure simulation and structural realism significantly improved with further spring discretization. Multi-spring configurations exhibited more distributed and physically realistic damage patterns, enhanced the simulation of energy dissipation mechanisms, and provided a more robust analytical foundation for assessing the performance of MIW in RC frames under complete tsunami inundation. While providing only slight enhancements in peak strength, the incorporation of four or five spring elements effectively captured the critical interaction effects between the infill and the surrounding frame that were neglected in the lower-resolution models, thus facilitating more precise and dependable structural evaluations under extreme loading conditions.

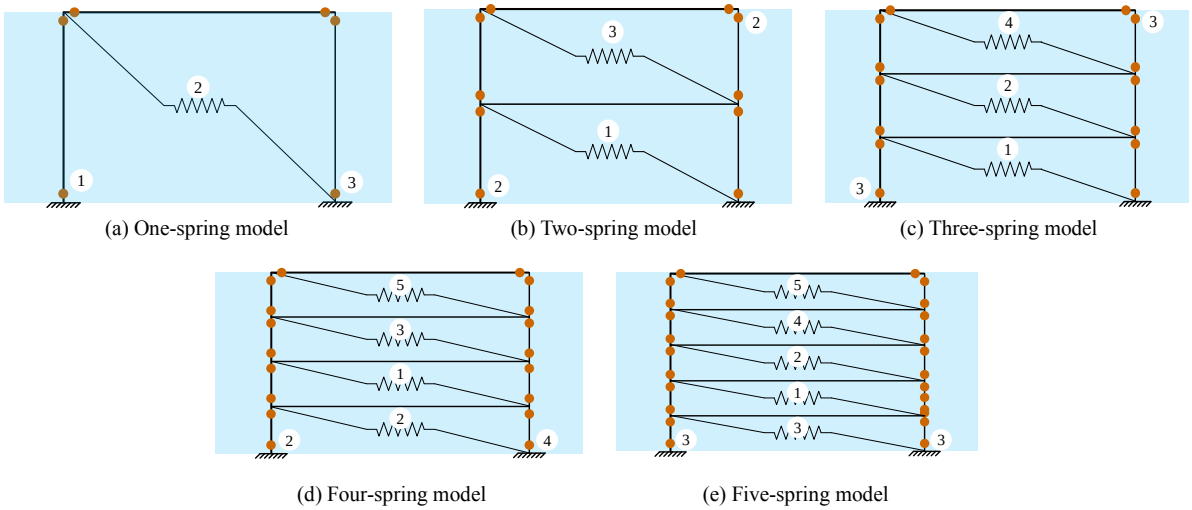

Figure 13. The failure mechanisms of the MIW models that were subjected to tsunami inundation depths of 1.00H

Table 2 presents a comparative analysis of the maximum lateral resistance derived from the MIW models with different degrees of spring discretization over four tsunami inundation depths: 0.25*H*, 0.50*H*, 0.75*H*, and 1.00*H*. A similar pattern was observed, whereby the lateral resistance often decreases with the increasing inundation depth, which can be attributed to a decrease in the effective wall area opposing the hydrodynamic pressures. The precision of these predictions is significantly affected by the quantity of the spring elements incorporated in the model. At a shallow inundation (0.25*H*), the one-spring structure considerably overestimated the lateral capacity, exhibiting a 52.5% inaccuracy due to its failure to replicate the vertical force gradient, thereby directing the load primarily through the front column. As the number of springs was increased, the difference decreased significantly. The four-spring model attained near-optimal concordance with the experimental benchmarks (2.5% inaccuracy). At intermediate inundation levels (0.50*H* and 0.75*H*), the three-spring to five-spring models reliably sustained prediction errors within ±5%, accurately reflecting the steady progression of load and wall-frame interaction. In contrast, the one-spring and two-spring models continued to exhibit differences in performance due to their limited vertical resolution. During complete inundation (1.00*H*), the hydrodynamic force was uniformly distributed along the wall height, which resulted in enhanced consistency across all models, with the one-spring model merely exhibiting a 2.4% inaccuracy. However, models with enhanced spring resolution were able to more accurately replicate nonlinear behavior and force redistribution, confirming their suitability for structural evaluation under various tsunami loading scenarios.

Table 2. A Comparison of the maximum lateral resistance of the MIW models under various tsunami inundation heights

Models	0.25H		0.50H		0.75H		1.00H	
	Max Resist (kN)	Error (%)	Max Resist (kN)	Error (%)	Max Resist (kN)	Error (%)	Max Resist (kN)	Error (%)
1-Spring	1,228.0	52.5	616.0	20.7	439.1	8.1	352.2	2.4
2-Springs	924.5	14.8	489.7	-4.0	370.2	-8.8	319.3	-7.1
3-Springs	858.6	6.6	487.0	-4.5	384.2	-5.4	329.5	-4.2
4-Springs	825.2	2.5	518.0	1.5	398.0	-2.0	339.2	-1.3
5-Springs	805.1	-	510.2	-	406.1	-	343.8	-

The failure modes derived from each configuration further emphasized the significance of inundation depth in influencing structural response. At low water levels, specifically 0.25H, failure was predominantly confined to the base of the frame, characterized by plastic hinge formation and spring yielding that was concentrated in the lower sections, particularly in one-spring and two-spring models. These configurations typically exhibited a frame-dominant mechanism, which inadequately utilized the infill wall and misrepresented the internal load transfer. With deeper inundation (0.50H and 0.75H), a rising quantity of the spring elements becomes submerged and activated, leading to an expanded damage progression throughout both the infill and the frame. Yielding occurred throughout several spring layers, with plastic hinges forming at different column heights, especially at the rigid link interfaces, indicating improved structural interaction. At the maximum inundation depth (1.00H), all spring segments were completely activated, resulting in uniform spring yielding and hinge formation that reflected true physical behavior under severe hydrodynamic loads. Multi-spring arrangements, especially those including four or five springs, effectively capture this complicated formation while facilitating a more realistic simulation of energy dissipation and load-sharing behaviors. These discoveries underscore that enhanced vertical discretization is not only essential for estimating strength, but is also essential for accurately simulating failure mechanisms, which is crucial for the design of tsunami-resistant RC frames with infilled masonry.

The main objective of this research is to propose a reliable and efficient model approach to analyzing the lateral response of MIWs under tsunami-induced hydrodynamic loads through a vertically discretized multi-spring approach. The analytical results of this investigation cannot be directly compared with prior experimental research, as no current studies have examined the same particular specimen under tsunami-induced loading conditions. The variations in RC frame configurations employed in prior investigations further limit direct comparability due to their effect on structural response. The proposed modeling framework is adaptable for MIWs with openings or irregular shapes by adjusting the distribution and strength of spring elements following local stiffness variations and material discontinuities. The concept includes rigid links between column parts to provide effective force transmission. This system is inherently extensible and can be used for multi-story structures. Regarding that tsunami-induced forces are often distributed continuously over the inundation depth, the multi-spring model can be utilized at each story level to accurately represent the localized interaction between MIWs and surrounding RC frames. The modeling approach depends on geometric and load distribution principles rather than material-specific factors; nonetheless, the real lateral resistance and failure modes are affected by masonry characteristics, including brick compressive strength and mortar shear capacity. The material properties determine the strength and stiffness of each spring, influencing the yield point and post-peak response. Consequently, precise calibration of spring properties, based on empirical data or computational values, is essential for accurately forecasting structural performance.

6. Conclusions

This study investigated the structural performance of masonry-infilled walls (MIWs) in reinforced concrete (RC) frame structures that had been subjected to tsunami-induced hydrodynamic loading, using the approach of multi-horizontal-spring-element modeling with the number of spring elements ranging from 1 to 5. The proposed model was calibrated against experimental data gleaned from Mehrabi et al. [3] and was extended to account for tsunami force distributions that varied across inundation depths. The findings of this research can be summarized as follows:

- The amount of vertical discretization in the MIW model, which can be achieved by increasing the number of nonlinear spring elements, was found to directly influence the precision of the global force-deformation responses and local failure mechanisms. The one-spring and two-spring models often overestimated lateral resistance and localized deformation within the RC frame. In contrast, models with three or more springs accurately reflected the vertical stress gradient; more effectively distributed the internal forces, and replicated the intricate failure sequences, including the sequential yielding of the infill layers and the formation of plastic hinges at the various elevations. This highlighted the significance of multi-spring discretization for accurate tsunami load simulation.
- The depth of tsunami inundation significantly influenced the structural responses. At shallow depths (e.g., 0.25H), low-resolution models significantly misrepresented the contribution of the infill and channel force transmission predominantly to the front column, leading to overestimates of the force estimations. As the inundation depth was increased (0.50H–1.00H), a larger segment of the wall became submerged, resulting in additional spring layers. This resulted in a transition from concentrated to spread damage processes that are characterized by failure mechanisms, which included multi-level infill yielding, hinge formation in both front and rear columns, and a more gradual post-peak degradation, particularly in the models featuring four or five spring elements.
- The one-spring model may demonstrate the most significant peak lateral resistance in some conditions. However, it did not accurately represent the real failure progression and energy dissipation behavior that was observed in the more comprehensive simulations. Although exhibiting slightly reduced peak resistance, the four-spring and five-spring models provided a more precise prediction of residual strength, failure mechanism, and post-peak behavior, which rendered them as more dependable for performance-based design and risk assessment in tsunami scenarios. The enhancement in global lateral resistance prediction levels off after the three spring elements. Currently, improvements in modeling accuracy, failure mechanisms, and the interaction between the MIW and RC frame persist. This convergence suggests that although three-spring models may provide sufficient accuracy for preliminary design, four-spring or five-spring models are more suitable for detailed analysis, especially in performance-based or retrofit evaluations for which understanding any localized damage is crucial.
- The findings endorsed the implementation of vertically discretized infill models within tsunami-resistant design approaches. The improved simulation of hydrodynamic force transfer, failure mechanisms, and frame–infill interaction ensures that essential behaviors, such as interface separation, spring yielding progression, and column hinging, are accurately simulated. These findings are crucial for formulating comprehensive analytic approaches and performance-based evaluation standards for low-rise to mid-rise structures that are situated in tsunami-prone coastal areas.

7. Declarations

7.1. Author Contributions

Conceptualization, P.F., A.R., and A.N.; methodology, P.F., N.T., and A.N.; software, S.T., J.P., and A.N.; validation, P.F., T.O., and N.T.; formal analysis, S.T. and J.P.; investigation, S.T., J.P., and A.N.; resources, P.F., N.T., and P.C.; data curation, P.F. and A.N.; writing—original draft preparation, P.F., A.N., N.T., S.P., and J.P.; writing—review and editing, P.F., N.T., T.O., A.R., and P.C.; visualization, A.R. and P.C.; supervision, A.R. and P.C.; project administration, P.F., S.T., and J.P.; funding acquisition, P.F., A.R., and P.C. All authors have read and agreed to the published version of the manuscript.

7.2. Data Availability Statement

The data presented in this study are available in the article.

7.3. Funding and Acknowledgements

This research was supported by the Fundamental Fund of Khon Kaen University from the National Science, Research and Innovation Fund (NSRF) of Thailand. The authors gratefully acknowledge this financial support.

7.4. Conflicts of Interest

The authors declare no conflict of interest.

8. References

[1] NOAA. (2005). Indian Ocean Earthquake and Tsunami: December 26, 2004. National Oceanic and Atmospheric Administration (NOAA), Silver Spring, United States. Available online: https://www.ngdc.noaa.gov/hazard/26dec2004.html (accessed on August 2025).

[2] USGS (2011). Magnitude 9.0 - Near the East Coast of Honshu, Japan. United States Geological Survey (USGS), Reston, United States Available online: https://www.strongmotioncenter.org/NCESMD/data/japan_11mar2011_54623utc/eqinfo.htm (accessed on August 2025).

[3] Mehrabi, A. B., Benson Shing, P., Schuller, M. P., & Noland, J. L. (1996). Experimental Evaluation of Masonry-Infilled RC Frames. Journal of Structural Engineering, 122(3), 228–237. doi:10.1061/(asce)0733-9445(1996)122:3(228).

[4] Kakaletsis, D., & Karayannis, C. (2007). Experimental investigation of infilled r/c frames with eccentric openings. Structural Engineering and Mechanics, 26(3), 231–250. doi:10.12989/sem.2007.26.3.231.

[5] Ozkaynak, H., Yuksel, E., Yalcin, C., Dindar, A. A., & Buyukozturk, O. (2014). Masonry infill walls in reinforced concrete frames as a source of structural damping. Earthquake Engineering and Structural Dynamics, 43(7), 949–968. doi:10.1002/eqe.2380.

[6] G. Asteris, P. (2012). Modeling of Infilled Frames With Openings. The Open Construction and Building Technology Journal, 6(1), 81–91. doi:10.2174/1874836801206010081.

[7] HOLMES, M. (1961). Steel Frames With Brickwork and Concrete Infilling. Proceedings of the Institution of Civil Engineers, 19(4), 473–478. doi:10.1680/iicep.1961.11305.

[8] Lee, S. J., Eom, T. S., & Yu, E. (2021). Investigation of Diagonal Strut Actions in Masonry-Infilled Reinforced Concrete Frames. International Journal of Concrete Structures and Materials, 15(1), 1–14. doi:10.1186/s40069-020-00440-x.

[9] El-Dakhakhni, W. W., Elgaaly, M., & Hamid, A. A. (2003). Three-Strut Model for Concrete Masonry-Infilled Steel Frames. Journal of Structural Engineering, 129(2), 177–185. doi:10.1061/(asce)0733-9445(2003)129:2(177).

[10] Crisafulli, F. J., & Carr, A. J. (2007). Proposed macro-model for the analysis of infilled frame structures. Bulletin of the New Zealand Society for Earthquake Engineering, 40(2), 69–77. doi:10.5459/bnzsee.40.2.69-77.

[11] Asteris, P. G., Chrysostomou, C. Z., Giannopoulos, I. P., & Smyrou, E. (2011). Masonry infilled reinforced concrete frames with openings. III ECCOMAS Thematic Conference on Computational Methods in Structural Dynamics and Earthquake Engineering (COMPDYN 2011), 26-28 May, 2011, Corfu, Greece.

[12] Dias-Oliveira, J., Rodrigues, H., Asteris, P. G., & Varum, H. (2022). On the Seismic Behavior of Masonry Infilled Frame Structures. Buildings, 12(8), 1146. doi:10.3390/buildings12081146.

[13] Galvão, L. F., & Alva, G. M. S. (2023). Structural analysis of RC infilled frames with participating masonry: a proposal procedure for multi-strut models. Revista IBRACON de Estruturas e Materiais, 16(4), e16409. doi:10.1590/S1983-41952023000400009.

[14] P.G. Asteris. (2008). Finite Element Micro-Modeling of Infilled Frames. Electronic Journal of Structural Engineering, 8, 1–11. doi:10.56748/ejse.894.

[15] Stavridis, A., & Shing, P. B. (2010). Finite-Element Modeling of Nonlinear Behavior of Masonry-Infilled RC Frames. Journal of Structural Engineering, 136(3), 285–296. doi:10.1061/(asce)st.1943-541x.116.

[16] Mohyeddin, A., Goldsworthy, H. M., & Gad, E. F. (2013). FE modelling of RC frames with masonry infill panels under in-plane and out-of-plane loading. Engineering Structures, 51, 73–87. doi:10.1016/j.engstruct.2013.01.012.

[17] Baloevic, G., Radnic, J., Matesan, D., Grgic, N., & Banovic, I. (2016). Comparison of developed numerical macro and micro masonry models for static and dynamic analysis of masonry-infilled steel frames. Latin American Journal of Solids and Structures, 13(12), 2251–2265. doi:10.1590/1679-78252520.

[18] Xi, K., & Liu, B. (2022). Seismic Performance and Finite Element Analysis of Reinforced Concrete Frames Considering a Masonry-Infilled Wall. Advances in Materials Science and Engineering, 2022, 1–16. doi:10.1155/2022/6832624.

[19] Li, Y., & Zeng, B. (2023). Modeling of masonry structures using a new 3D cohesive interface material model considering dilatancy softening. Engineering Structures, 277, 115466. doi:10.1016/j.engstruct.2022.115466.

[20] Ye, B., Su, Y., Chen, X., Zhu, D.-Z., & Pan, P. (2025). Seismic Performance of Unreinforced Masonry Wall Strengthened with Hybrid Basalt-Pe Fibers Engineered Cementitious Composites. SSRN, 1-45. doi:10.2139/ssrn.5367796.

[21] Yeh, H. (2007). Design Tsunami Forces for Onshore Structures. Journal of Disaster Research, 2(6), 531–536. doi:10.20965/jdr.2007.p0531.

[22] FEMA P-646. (2019). Guidelines for Design of Structures for Vertical Evacuation from Tsunamis. Prepared for Federal Emergency Management Agency. Applied Technology Council, Redwood City, United States.

[23] Lukkunaprasit, P., Thanasisathit, N., & Yeh, H. (2009). Experimental Verification of FEMA P646 Tsunami Loading. Journal of Disaster Research, 4(6), 410–418. doi:10.20965/jdr.2009.p0410.

[24] Foytong, P., Ruangrassamee, A., & Lukkunaprasit, P. (2013). Correlation analysis of a reinforced-concrete building under tsunami load pattern and effect of masonry infill walls on tsunami load resistance. IES Journal Part A: Civil and Structural Engineering, 6(3), 173–184. doi:10.1080/19373260.2012.756125.

[25] Cavaleri, L., Ciraolo, G., Ferrotto, M. F., La Loggia, G., Lo Re, C., & Manno, G. (2020). Masonry structures subjected to tsunami loads: Modeling issues and application to a case study. Structures, 27, 2192–2207. doi:10.1016/j.istruc.2020.08.033.

[26] Del Zoppo, M., Wijesundara, K., Rossetto, T., Dias, P., Baiguera, M., Di Ludovico, M., Thamboo, J., & Prota, A. (2021). Influence of exterior infill walls on the performance of RC frames under tsunami loads: Case study of school buildings in Sri Lanka. Engineering Structures, 234, 111920. doi:10.1016/j.engstruct.2021.111920.

[27] Belliazzi, S., Lignola, G. P., & Palermo, D. (2025). Simplified structural analysis framework for buildings under combined earthquake and tsunami loads. Structures, 77, 109206. doi:10.1016/j.istruc.2025.109206.

[28] Asad, M., Thamboo, J., Zahra, T., & Thambiratnam, D. P. (2025). Mitigating damages to infill walls under combined in-plane and out-of-plane loadings using a spider web-inspired strengthening strategy: Numerical analyses. Engineering Structures, 323, 119297. doi:10.1016/j.engstruct.2024.119297.

[29] ASCE/SEI 7-22. (2021). Minimum Design Loads and Associated Criteria for Buildings and Other Structures. American Society of Civil Engineers (ASCE), Reston, United States. doi:10.1061/9780784415788.

[30] FEMA P55. (2011). Coastal Construction Manual. Federal Emergency Management Agency (FEMA), Washington, United States.

[31] City and County of Honolulu (CCH). (2021). Chapter 16: Building Code. Department of Planning and Permitting of Honolulu, Hawaii, United States.

[32] Foytong, P., Ruangrassamee, A., Lukkunaprasit, P., & Thanasisathit, N. (2015). Behaviours of reinforced-concrete building under tsunami loading. IES Journal Part A: Civil & Structural Engineering, 8(2), 101–110. doi:10.1080/19373260.2015.1013998.

[33] ASCE. (2023). Seismic Evaluation and Retrofit of Existing Buildings. American Society of Civil Engineers (ASCE), Reston, United States. doi:10.1061/9780784416112.

[34] Mostafaei, H., & Kabeyasawa, T. (2004). Investigation and analysis of damage to buildings during the 2003 Bam earthquake. Bulletin of Earthquake Research Institute, University of Tokyo, 79, 107-132.

[35] Fritz, H. M., Borrero, J. C., Synolakis, C. E., & Yoo, J. (2006). 2004 Indian Ocean tsunami flow velocity measurements from survivor videos. Geophysical Research Letters, 33, L24605. doi:10.1029/2006GL026784.

[36] Foytong, P., Ruangrassamee, A., Shoji, G., Hiraki, Y., & Ezura, Y. (2013). Analysis of Tsunami Flow Velocities during the March 2011 Tohoku, Japan, Tsunami. Earthquake Spectra, 29(1_SUPPL), 161–181. doi:10.1193/1.4000128.